A NEW METHOD FOR SUB-PIXEL SNOW-COVER MAPPING USING HYPERSPECTRAL IMAGERY – FIRST RESULTS

R. Solberg
Norwegian Computing Center, P.O. Box 114 Blindern, N-0314 Oslo, Norway
Phone: +47 2285 2500, Fax: +47 2269 7660, E-mail: rune.solberg@nr.no

Abstract

Most methods applied for snow-cover mapping classify each pixel into snow and no-snow. On the other side, a sub-pixel method classifies snow into several coverage classes or onto a continuous scale. If frequent mapping is required, only low and medium spatial resolution sensors are available (200-1000 m range). Classifying pixels into snow and no-snow only may be sufficient for large-scale applications. The method presented here intends to solve the problems of the current linear reflectance-to-snow-coverage sub-pixel algorithm. It gives a fast and very accurate estimate for the actual snow cover at the sub-pixel level. The method is in particularly useful for hyperspectral data. The method predicts local end-member spectra for snow and bare ground for each pixel. Vegetation end-members are predicted using a vegetation map made from another satellite image and a vegetation development model. Furthermore, a local snow end-member-spectrum predictor is used to predict a spectrum, which matches the development stage of the snow. The predictors also compensate for terrain relief effects while generating the actual end-member spectra. The prior information and the predictors allow the number of possible end-members for each pixel to be very low. An iterative algorithm is proposed in order to unmix two and three class component spectra for the prediction of the areal contribution of each class. The method has been applied to field measured spectra. Further experiments are ongoing for airborne DAIS-7915 hyperspectral data covering the Heimdalen test site in Jotunheimen, Norway. The spatial resolution of the DAIS data is reduced to 250 m simulating a medium-resolution sensor. The preliminary results show that the new method gives higher accuracy and reasonable computation time. However, further assessment on larger data sets is necessary to make a full evaluation of the method.

Introduction

Seasonal snow cover has an extent during the winter months of 30-50 million km^2. This results in a substantial impact on climate processes, weather and the life in general of people living within this area. Seasonal snow cover is a significant water resource in many countries supplying electricity and freshwater. It is also a source of avalanches and floods. Its importance combined with its huge extent resulted very early in the history of remote sensing in snow-cover monitoring applications by satellite.

A large range of methods has been used for snow-cover mapping. These include classical approaches applying statistical supervised classification (1 and 2) and unsupervised classification using clustering (e.g., see 3). Hybrid methods combining the two approaches have also been developed (4). An alternative approach is to apply physically-based methods (e.g., see 5). This is very common within meteorology (6), and has also been the approach when developing the MODIS algorithm (7), which is part of the USA's global climate monitoring system.

All the above-mentioned algorithms are snow/no-snow methods classifying a pixel into either snow or no-snow. Alternatively, sub-pixel methods may be used, which classify each pixel into one of several coverage classes or onto a continuous scale. If frequent mapping is required, which is the usual case during the snowmelt season, only medium and low spatial resolution sensors are available (200-1000 m range). Classifying pixels into only snow and no-snow may be sufficient for large-scale applications, like global snow-cover monitoring for environmental applications. How-

ever, for medium and small-scale applications, like mapping catchments for hydropower production, or high-precision large-scale mapping, more exact information about the actual snow coverage inside a pixel is needed.

The need for higher accuracy resulted in the invention, by Norwegian users, of a simple algorithm for sub-pixel snow-cover mapping using NOAA AVHRR data already in the beginning of the 1980ies (8 and 9). The method is based on the assumption that there is a linear relationship between snow coverage and measured reflectance. When this relationship is established, it is an easy task to classify each pixel into snow-cover percentage or a coverage category. In (9), four categories were used. The relationship is established by using training areas or interpretation of a histogram of the image. A population of 100% snow covered pixels is identified and determines the reflectance for 100% snow coverage. A corresponding procedure is followed for 0% snow coverage. The method has been applied operationally in Norway since it was developed, and has also been used in Canada (10). The method has later been extended with automatic training (11), automatic geocoding and automatic cloud detection.

A relatively new approach to the problem of measuring snow at sub-pixel level is linear spectral unmixing. This is particularly suited for sensors having a high number of bands, imaging spectrometers, but it is also possible to use sensors like Landsat TM. Linear spectral unmixing assumes that a pixel is composed of several different classes, or end-members, and tries to estimate the aerial coverage of each class. Hence, the method does not rely on the assumption of one "background class" like the method described above. In (12), spectral unmixing for snow classification using a linear mixture model is introduced. The actual accuracy of the classification using spectral unmixing, was studied by (13) for an area in Mammoth Mountain in Sierra Nevada, California. The AVIRIS airborne spectrometer was used, and the actual snow cover was determined from aerial photography. The agreement between the snow cover map generated by spectral unmixing and the aerial photography was found to be 92% for areas of low relief and little shade. The agreement fell to about 71% in areas that were extensively shaded.

A disadvantage of spectral unmixing, as applied in (12) and (13), is that the method is supervised. The spectral end-members have to be identified manually by training. In (15), a method for unsupervised spectral unmixing is proposed. The method determines end-members automatically and then compares them to a spectral library to estimate the mixture of each pixel. The first step is to use a classification tree to fragment the image into distinct land and cloud cover classes (16). The dimensionality and number of end-members are then determined for each fragment using principal component analysis. Each fragment is unmixed with all end-members sets located on its convex hull, and the best set is selected. The end-member spectra are corrected for the atmosphere using a radiative transfer model, and the end-members are then identified in a spectral library. The final snow cover is then determined from the best mixture model taking into account possible end-member impurities. The method was tested on Landsat TM data and found to have similar accuracy to aerial photography.

- The motivation for the new method presented here is that:
- Sub-pixel accuracy is a requirement for small-scale applications
- Sub-pixel accuracy is an advantage for large-scale applications
- The classical linear reflectance-to-snow-coverage method is far from accurate enough
- Classical linear spectral unmixing is a supervised method needing manual intervention
- The above-mentioned proposal for unsupervised classification is computationally demanding
- Spectral unmixing may in general give very inaccurate results since many combinations of end-members may give the same resulting spectrum

The new method presented here intends to solve or limit the above-mentioned problems. The method is useful, in particular, for hyperspectral data. It applies a new iterative spectral unmixing algorithm in the last step. The number of spectra to unmix is limited to a minimum by a priori in-

formation. Topographic effects are compensated for. The method applies local end-member spectra, which are generated for each individual pixel by special predictors for snow, vegetation and other bare-ground classes.

The method has been tested on field-measured spectra and is currently evaluated on airborne DAIS-7915 hyperspectral data covering the Heimdalen test site in Jotunheimen, Norway. DAIS 7915 (Digital Airborne Imaging Spectrometer) is a 79 bands spectrometer. Together with the airborne synthetic aperture radar EMISAR, these sensors comprise the European Airborne Sensing Capabilities (EARSeC) developed as an initiative by the European Union. The spectrometer was built by Geophysical Research corp. (GER), USA, and has been improved by Deutsches Zentrum für Luft- und Raumfahrt e.V. (DLR), Germany. Due to requirements for very accurate calibration, a calibration laboratory was built at DLR. Two flight periods were accomplished in 1997 and 1998 as part of a European-wide campaign.

The data were acquired in June 1998 as part of the DAIS-LSF'98 airborne campaign and cover most of a 100 km^2 catchment. Very accurate snow-cover data were obtained at the same time from aerial photographs. A vegetation map was generated from Landsat TM data, and an accurate DEM was generated from the aerial photographs. Calibration end-member spectra were measured in the field using a FieldSpec portable spectrometer. The spatial resolution of the DAIS data was reduced to 250 m simulating a medium resolution sensor. The new method and the classical linear reflectance-to-snow-coverage method are applied to the data set.

The Snow-Cover Classification Method

A brief overview of the approach proposed will be presented followed by a detailed description. The method comprises five fundamental components: accurate prior data about the area to map, models for the spectral development of the end-members possibly present, radiometric correction for terrain effects, radiometric atmospheric correction and a new iterative spectral unmixing algorithm for the retrieval of the actual snow coverage within the pixel. The prior data comprises an end-member class map for the bare ground and a digital terrain model. The terrain model is only required when radiometric terrain correction is needed. The spectra for snow, vegetation and to some degree other bare ground classes change more or less all the time, with the largest changes present during the melting season when the snow metamorphosis develops fastest and the vegetation turns green. Predictors for the spectra have been developed, which limit the number of end-member spectra to decompose for a given pixel to a minimum. The decomposition is done by the new spectral unmixing algorithm.

End-member Class Map

The classical reflectance-to-snow-cover sub-pixel mapping algorithm assumes a single bare-ground spectrum for the whole image. The use of linear spectral unmixing by several authors compensates for this by assuming many possible classes present and tries to estimate the actual classes by spectral decomposition. However, due to the temporal development of the classes, an extreme number of end-members must be used to cover all the spectra that may be present. With very many spectra to unmix, there are often several solutions giving the observed spectrum. In particular, the snow area searched may be wrongly estimated. Here, it is proposed to use an end-member class map giving prior information limiting the number of classes to unmix for each pixel. By the term *end-member class* is here meant a group of end-members representing one thematic class, like the end-member class grass, which is represented by a set of different spectra all representing various development stages of grass.

For the geographical area to monitor, an end-member class map has to be generated. The map, $M_{e,}$, can be expressed as:

$$M_e(x, y) = \{S_c \mid c \text{ is a class end-member at location } (x, y)\} \quad (1)$$

where (x, y) is the geographical position (covered by a pixel) and S_c is the set of all possible end-member spectra for class c. In order to reduce the total number of spectra, models will be used to generate the spectra in S_c for vegetation. Furthermore, M_e is in practice implemented as a map of references to a spectral library of actual and model end-members (see Figure 1).

In order for the method to be of interest for medium and large-scale operational applications, the end-member class map must be generated with minimal human intervention. The map may very well be made by classification of a satellite image of the same area acquired during snow-free conditions in the summer. This approach is actually much better than using a regular vegetation map made by other means because it is the spectral classes that are needed, not the actual vegetation classes. As long as two different vegetation classes have the same spectrum, they can be treated as one end-member here. Additionally, the usual generalisation present in a vegetation map is a deficit for this application. It is proposed to use an unsupervised classification method, preferably one that also does not need to know the number of classes to cluster. ISODATA (17) has shown to work well for the task given here. The clustering algorithm also takes into account the data distribution within a cluster to determine whether it is composed of more than one class.

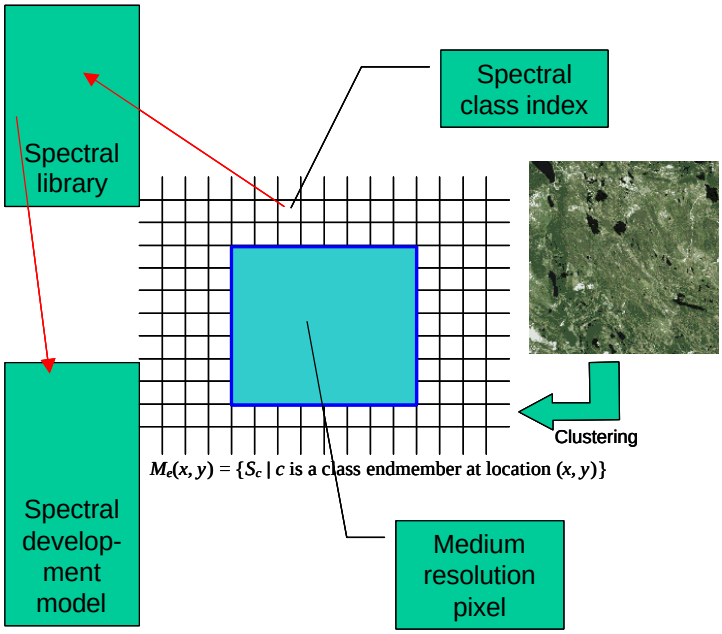

Figure 1: Conceptual overview of the spectral end-member class map.

Spectrum Predictors

The situation we have for snow and vegetation spectra is a continuous development from an initial spectrum to a final spectrum during the winter-spring season. The change over time represents a continuous function. However, the gradient will in general not be a constant, but vary with the changes in the growing conditions for vegetation and incoming energy and precipitation for snow. If we represent a reflectance spectrum by a vector, the situation can be described as follows:

$$\boldsymbol{s}_f = \boldsymbol{s}_i \, \boldsymbol{m} \tag{2}$$

where $\boldsymbol{s}_f$ is the final spectrum, $\boldsymbol{s}_i$ the initial spectrum and $\boldsymbol{m}$ the modification spectrum. Intermediate spectra can be generated by scaling the modification spectrum:

$$\boldsymbol{s} = \boldsymbol{s}_i \, \boldsymbol{m} \, r \tag{3}$$

where $\boldsymbol{s}$ is an intermediate spectrum and r is the corresponding scaling factor within the range [0,1]. The path of $\boldsymbol{s}$ in the hyperspectral space, for all values of r successively from 0 to 1, represents the

development history of the spectrum ***s***. *r* is a function of time, *r*(*t*), but in general not a linear function as commented above. Hence, it is not straightforward to predict *r*. The most fruitful approach would probably be to estimate the effective time, t_e, which is linearly dependent on the product of time and the development factors, like the air temperature for snow, and the air temperature and soil moisture for vegetation. (This approach corresponds to the use of degree-days in snow hydrology modelling.) However, here a more direct (and safe) approach is applied by measuring features in the mixed spectrum with a magnitude which is proportional to the development stage (i.e., *r).*

Vegetation Spectra

The most characteristic feature in a vegetation spectrum is the red-edge, a very steep gradient in the near infrared (e.g., 18). The magnitude of the feature is proportional to the fraction of green vegetation (green area) covering the field of view. This means that if the feature is almost non-disturbed in the mixture spectrum, it can be used as an indicator of the development stage of the vegetation part of the mixed spectrum. The red edge is a local phenomenon in the spectrum (covering an interval of about 100 nm). The feature should be non-disturbed as long as there are no steep gradients in the other spectra it will mix with.

A gradient operator for the red edge, G_{re}, is here defined, corresponding to a gradient over the interval 650-750 nm. There is a linear relationship between *r* and G_{re}:

$$r_v = a_v G_{re,v} + b_v, \tag{4}$$

where *v* is an index to the vegetation end-member class in the spectral library. Hence, there is one such relationship for each vegetation end-member class.

Snow Spectra

A snow spectrum has typically high reflectance values in the visual part with the highest values around 500 nm where the reflectance is 90-100% (5). It decreases in the near infrared, most steeply between 1200 and 1500 nm. There are a couple of peaks around 1800 and 2250 nm. However, the reflectance in the short-wave infrared varies a great deal with grain size. The 1800 nm peak may have a reflectance of about 40% for a grain size of 50 µm, while it is reduced to about 3% for a grain size of 1000 µm. There is also a reduction in visible wavelengths for reduced grain size, however, the mentioned grain size reduction amounts to a reflectance reduction of only about 5% at 500 nm. What may reduce the reflectance much more at visual wavelengths are the presence of dark particles, impurities, in the snow (like wind-transported soil particles). The phenomenon typically takes place late in the snowmelt season with a mixture of bare ground and snow cover, and will usually increase with time until the snow has gone. The concentration of impurities is difficult to predict by modelling, but could be predicted based on a time series of data through several seasons and registering the frequency and level of the phenomenon locally. Impurities will not be modelled explicitly here, but in general taken into account by overcompensating for increased grain size in visual wavelengths.

One of the steepest gradients in the snow spectrum is around 1400 nm. The reflectance is reduced from about 70% to 10% for a grain size of 50 µm, and from about 20% to 1% for a grain size of 1000 µm. This spectral feature will here be nicknamed the *NIR edge*. As for the red edge of vegetation, if the feature is relatively non-disturbed in the mixture spectrum, it can be used as an indicator of the metamorphosis stage of the snow. Comparison with the typical spectra for vegetation, rock and soil shows that there are no other steep features in the 1400 nm region.

A gradient operator for the NIR edge, G_{ire}, is defined, corresponding to a gradient over the interval 1350-1450 nm. The linear relationship between *r* and G_{re} is established:

$$r_s = a_s G_{ire,s} + b_s, \tag{5}$$

where *s* indicates the end-member class snow in the spectral library.

Rock and Soil Spectra

The vegetation cover decreases with elevation, and high-mountain areas are typically covered with only a mixture of rock and bare soil. Rock is also present within vegetated areas, and soil may also be visible, especially in the early part of the vegetation-growing season and in areas temporally covered with water. Minerals (rocks and components of soil) have very characteristic spectra in the infrared part of the spectrum (in particular at longer wavelengths) (19). At visible and near-infrared wavelengths, the spectra are typically much smoother with very few unique features. Rock and soil spectra are typically very stable over time, however, they are influenced by moisture (20). The effect of water is typically to reduce the reflectance in visible and at short-wave infrared wavelengths. It may be reduced as much as 40% in the near infrared, depending on the amount of water. For soil, organic matter also reduces the reflectance effectively, however, the amount of organic matter is assumed to be constant over time here.

In the model proposed to use here, it will not be discriminated between soil and rock. The effect of moisture is proposed to be modelled by a mixture of dry soil/rock and completely wet soil/rock. This is of course not physically true, but should be sufficient here since we are only interested in the total surface area covered by soil/rock. This gives the following spectral model:

$$\boldsymbol{s}_{s/r} = a_d \boldsymbol{s}_{ds/r} + a_w \boldsymbol{s}_{ws/r}, \tag{6}$$

where $\boldsymbol{s}_{s/r}$ is the resulting spectrum, $\boldsymbol{s}_{ds/r}$ is the spectrum of dry soil/rock, $\boldsymbol{s}_{ws/r}$ is the spectrum of wet soil/rock, a_d is the fractional area of dry soil/rock and a_w is the fractional area of wet soil/rock. In practice, these spectra may be established by measuring a lot of dry and wet soil and rock samples and, then, determining the mean dry and mean wet spectrum. As for vegetation, the types of soil and rocks will vary between different geographical regions. Hence, soil and rock spectra used in the spectral library should not be treated uniquely, but should be selected according to the geographical region.

The Algorithm

The description of the algorithm proposed is here limited to a combination of the two end-member classes snow and vegetation. The two classes have spectra varying with time as their characteristics changes through the season. The algorithm assumes that the sub-pixel spectral contribution of snow and vegetation can be combined in a linear way according to the two classes' areal contribution to the pixel's total reflectance:

$$R(l) = a_s S(l) + a_v V(l) \tag{7}$$

The equations applied in the iterative algorithm are derived from this equation. The algorithm is defined as follows:

0. Initially, use a priori spectra for snow and vegetation, $\hat{S}(l)^{(0)}$ and $\hat{V}(l)^{(0)}$
1. Estimate the snow fraction at λ_{as}: $\hat{a}_s^{(i)} = \dfrac{R(l) - \hat{V}(l)^{(i)}}{\hat{S}(l)^{(i)} - \hat{V}(l)^{(i)}}$
2. Estimate the vegetation reflectance at $\lambda_{rededge}$: $\hat{V}(l)^{(i)} = \dfrac{R(l) - \hat{a}_s^{(i)} \hat{S}(l)^{(i)}}{1 - \hat{a}_s^{(i)}}$
3. Identify a better approx. to the vegetation spectrum, $V(\lambda)$, based on the red-edge gradient, $G_{rededge}$
4. Estimate the vegetation fraction at λ_{av}: $\hat{a}_v^{(i)} = \dfrac{R(l) - \hat{S}(l)^{(i)}}{\hat{V}(l)^{(i)} - \hat{S}(l)^{(i)}}$
5. Estimate the snow reflectance at $\lambda_{NIRedge}$: $\hat{S}(l)^{(i)} = \dfrac{R(l) - \hat{a}_v^{(i)} \hat{V}(l)^{(i)}}{1 - \hat{a}_v^{(i)}}$

6. Identify a better approximation to the snow spectrum, $S(\lambda)$, based on the NIR-edge gradient, G_{NIRedge}

7. IF > 2 iterations AND $\frac{\left|\Delta\hat{a}_s^{(i)}\right| + \left|\Delta\hat{a}_v^{(i)}\right|}{2} < \Delta\hat{a}_{\max}$ THEN stop ELSE goto Step 1

The a priori spectra selected in Step 0 are typical spectra expected for the current time of the season. Good a priori spectra estimates assure quicker convergence. Steps 1-7 represent a loop making an iterative estimation of the snow and vegetation spectra and their areal contribution. A new estimate of the snow fraction is found in Step 1 at wavelength λ_{as} where the spectral contribution from vegetation is rather small and varies little with the development of the vegetation (see Figure 3). The new estimate of the snow fraction is applied in Step 2 for making an estimate of the vegetation's reflectance at the wavelength region λ_{rededge} where the vegetation has the characteristic so-called *red edge*. A better approximation to the actual vegetation spectrum is predicted from the red-edge gradient G_{rededge} in Step 3. Similarly to Step 1 for snow, the vegetation fraction at λ_{av} is estimated in Step 4, now applying the new estimate of the vegetation spectrum. The steep reduction of the reflectance for snow in the near infrared is here nicknamed the *NIR edge*. The snow reflectance is estimated for the spectral region λ_{NIRedge} in Step 5. The spectral characteristics here of snow, G_{NIRedge}, are used to predict a better spectrum for the snow. Step 7 determines if the iterations should continue or stop. At least two iterations are run, and the algorithm stops if the changes of the areal estimates of snow and vegetation change less than a given value between two iterations (the maximum error accepted).

Experiments

The Data Set

The test area, Heimdalen, is located in the Jotunheimen mountain area in Norway (9.0° E; 61.4° N). The area is of about 100 km^2 with an elevation range of 1050-1840 m a.s.l. The area is free of tall vegetation except for some birch in the lowest locations (not within applied data).

Heimdalen was covered by DAIS 7915 image acquisition on 21 June 1998 between about 8:13 and 9:31 GMT (about 9:30-10:50 true solar time). The imaging spectrometer has 79 bands covering the spectral range 0.4-12.6 μm. Some sensor characteristics are given in Table 1. The dynamic range is 15 bits. The sensor scans with a swath angle of ±26° generating lines of 512 pixels. The flight altitude was fixed such that the mean pixel size was 5×5 m^2. Ten stripes, of a total length of 90 km of data with a swath with of 2.5 km, were acquired. Seven stripes were oriented with flight direction parallel to the solar plane, thereby minimizing anisotropic reflectance, while three stripes were flown perpendicular to the solar plane in order to maximize the anisotropic reflectance.

Table 1: Spectral characteristics of DAIS 7915

Wavelength interval (μm)	Number of bands	Bandwidth
0.4-1.0	32	15-30 nm
1.5-1.8	8	45 nm
2.0-2.5	32	20 nm
3.0-5.0	1	2.0 μm
8.0-12.6	6	0.9 μm

A digital elevation model (DEM) was generated for the whole area based on 1:40,000 scale aerial photos acquired under snow-free conditions on 15 August 1998. The 14 photographs from two stripes were scanned, and a block of stereo models generated using a digital photogrammetric workstation. Automatic co-registration of image pairs was done, followed by manual absolute orientation

using ground control points. Terrain elevation was then derived for 5×5 m^2 pixels with a height accuracy of about 1 m.

In order to get an accurate map of the snow cover, aerial photographs were acquired simultaneously with the DAIS data. A similar flight plan and data processing procedure as for the DEM generation was followed. The result was a 1 m spatial resolution orthophoto covering the whole study area.

A snow mask was derived from DAIS band 25 (center wavelength 912 nm) and controlled against the orthophoto. The orthophoto could also have been used, but this approach was avoided in order to eliminate co-registration errors affecting the evaluation of the classification accuracy.

A field campaign was carried out during the image acquisition. Two field teams measured the snow parameters grain size, wetness, density, temperature and the spectral reflectance by a FieldSpec spectro-radiometer covering the spectral range 350-2500 nm. In addition the air temperature was measured. The snow parameters were measured at nine different point locations. Complementary ground temperature measurements were done at seven snow-free locations using a digital thermometer with physical ground contact and an IR thermometer with spectral coverage 7-16 µm. The location of each point was determined by GPS.

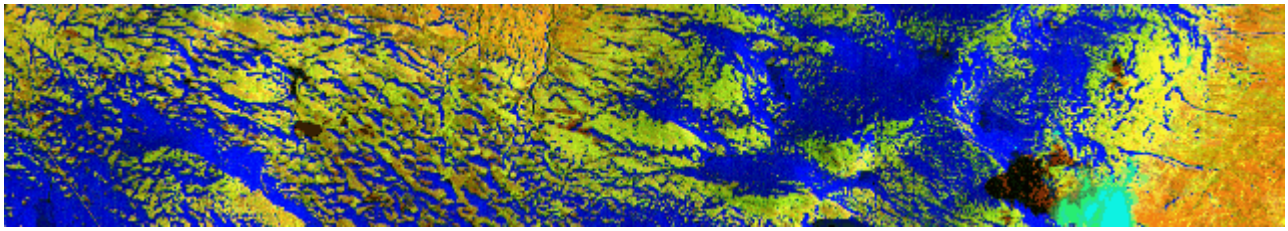

Figure 2: One of the DAIS image stripes showing the scattered snow conditions. A cloud and its cloud shadow is visible to the lower right.

Results

The first results of the experiment presented here are limited to the application of the field-measured spectra. A series of combinations of snow and vegetation spectra simulating different areal contribution of the two classes has been made. The iterative algorithm has then been applied to unmix the two spectra while estimating the sub-pixel fractional area of each class. The results show that it was possible to predict the fractions with an error of typically < 3%. An example of field-measured spectra and their linear combination with 50% fractional area each is shown in Figure 3. The three spectral regions with large spikes are due to sensor noise.

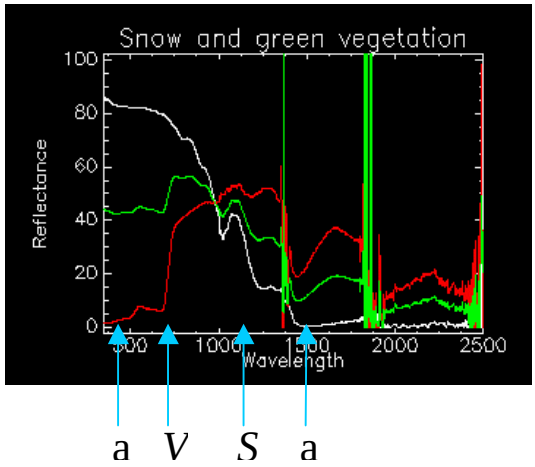

Figure 3: *Two typical snow and vegetation spectra are shown together with the combined spectrum. The spectral regions applied in the iterative algorithm are indicated with the arrows and associated variables estimated using these regions (see the description of the algorithm).*

Discussion And Conclusions

The first results presented here are limited to laboratory experiments with linear combinations of field-measured spectra. The results so far are very promising indicating that the iterative spectral unmixing algorithm is able to reasonably correctly predict the actual fraction of snow within a pixel.

However, there are several limitations to the experiment that makes it impossible to assess the true performance of the algorithms in operational applications. First of all, the algorithm tested so far is only the two-class version. A three-class version will have to include the combined class rock/soil. The most important error sources include spectral variations due to the topography, natural spectral variability not accounted for in the spectral model/spectral library, presence of other ground classes and spectral variability due to the atmosphere. The topography and atmosphere is corrected for in the method proposed, however, the performance of these corrections will always be limited by the accuracy of the digital terrain model available and the accuracy of the atmospheric model.

The method also builds on some assumptions that it has not been possible to verify so far. It is assumed that there is only one dominating spectrum for each of the end-member classes snow, vegetation and soil/rock within a pixel. Additionally, it is assumed that the anisotropic effects of snow are small, and it is assumed that the soil and rock can be treated as a combined spectral end-member.

The current experiment is followed by an experiment evaluating the method for 250×250 m^2 pixels based on the DAIS data within the spectral range 0.4-2.5 μm. DAIS pixels of 5×5 m^2 are aggregated into the larger pixels. The DAIS data is also used for assessing the performance of the algorithm on the 250×250 m^2 pixel data. Original data is classified by standard methods into snow and no-snow, and the fraction of each class is calculated for the 250×250 m^2 pixel data making it possible to accurately assess the performance of the method. The aerial photos are similarly used as a ground truth to assess the accuracy.

Acknowledgements

The author would like to thank the field team for their contributions and for their very enthusiastic attitude during a long waiting period before the weather allowed data acquisition. Many thanks also go to the flight teams (DAIS and Fotonor) for excellent execution of their respective flight plans. The work was sponsored with data and support from the TMR EU research programme via DLR and through the SNOWTOOLS project funded by EU under the contract ENV4-CT96-0304.

References

M.F. Baumgartner and A. Rango. 1995: A microcomputer-based alpine snow-cover analysis system (ASCAS). *Photogrammetric Engineering & Remote Sensing*, Vol. 61, No. 12, pp. 1475-1486.

A.N. Swamy and P.A. Brivio. 1996: Hydrological modeling of snowmelt in the Italian Alps using visible and infrared remote sensing. *International Journal of Remote Sensing*, Vol. 17, No. 16, pp. 3169-3188.

A.R. Harrison and R.M. Lucas. 1989: Multi-spectral classification of snow using NOAA AVHRR imagery. *International Journal of Remote Sensing*, Vol. 10, pp. 907-916.

H. Xu, J.O. Bailey, E.C. Barrett and R.E.J. Kelly. 1993: Monitoring snow area and depth with integration of remote sensing and GIS. *International Journal of Remote Sensing*, Vol. 14, pp. 3259-3268.

J. Dozier. 1989: Spectral signature of Alpine snow cover from Landsat Thematic Mapper. *Remote Sensing of the Environment*, Vol. 28, pp. 9-22.

L.A. Breivik, S. Eastwood, Ø. Godøy, J. Sunde and C. Ulstad. 1997: Satellite Derived Sea Ice and Sea Surface Temperatures (SST) at DNMI. Status Report from March 1997, DNMI Research Note no. 4, Norwegian Meteorological Institute, Oslo, April 9, 1997.

G.A. Riggs, D.K. Hall and V.V. Salomonson. 1994: A snow index for the Landsat Thematic Mapper and Moderate Resolution Imaging Spectroradiometer. Proceedings of the International Geoscience and Remote Sensing Symposium (IGARSS), 8-12 August 1994, Pasadena, California, USA, pp. 1942-1944.

Østrem, T. Andersen and H. Ødegaard. 1979: Operational use of satellite data for snow inventory and runoff forecasting, satellite hydrology. Proceedings of Pecora Symposium, June 1979, American Water Resources Association, pp. 230-234.

T. Andersen. 1982: Operational snow mapping by satellites, Hydrological aspects of alpine and high mountain areas. Proceedings of the Exeter symposium, July 1982, IAHS publ. no. 138, pp. 149-154.

S. Ferner and I. Sutherland. 1987: The utility of computer-processed NOAA imagery for snow cover mapping and streamflow simulation in Alberta, Large scale effects of seasonal snow cover. Proceedings of the Vancouver symposium, August 1987, IAHS publ. no. 166, pp. 173-184.

R. Solberg and T. Andersen. 1994: An automatic system for operational snow-cover monitoring in the Norwegian mountain regions. Proceedings of International Geoscience and Remote Sensing Symposium (IGARSS), Pasadena, California, USA, 8-12 August 1994, pp. 2084-2086.

A.W. Nolin. 1993: Radiative heating in alpine snow. Ph.D. Theses, University of California, Santa Barbara, September 1993.

A.W. Nolin. 1994: Snowcover mapping with the Airborne Visible/Infrared Imaging Spectrometer. Proceedings of International Geoscience and Remote Sensing Symposium (IGARSS), Pasadena, California, USA, 8-12 August 1994, pp. 2081-2083.

A.W. Nolin. 1995: Mapping fractional snow covered area and sea ice concentrations. First Moderate Resolution Imaging Spectroradiometer (MODIS) Snow and Ice Workshop, September 13-14, NASA Conf. Publ. 3318, pp. 39-49.

W. Rosenthal. 1996: Estimating alpine snow cover with unsupervised spectral unmixing. Proceedings of the International Geoscience and Remote Sensing Symposium (IGARSS), 27-31 May 1996, Lincoln, Nebraska, USA, pp. 2252-2254.

W. Rosenthal and J. Dozier. 1996: Automated mapping of montane snow cover at subpixel resolution from the Landsat Thematic Mapper. *Water Resources Research*, Vol. 32, No. 1, pp. 115-130.

A.K. Jain and R.C. Dubes. 1988: Algorithms for Clustering Data, Prentice Hall.

B.N. Rock, J.E Vogelmann, D.L. Williams, A.F. Vogelmann and T. Hoshizaki. 1986: Remote detection of forest damage. *BioScience*, Vol. 36, pp. 439-445.

A.F.H Goetz. 1989: Spectral remote sensing in geology. In: G. Asrar (Ed): Theory and applications of optical remote sensing, John Wiley and Sons, pp. 491-526.

J.R. Irons, R.A. Weismiller and G.W. Petersen. 1989: Soil reflectance. In: G. Asrar (Ed): Theory and applications of optical remote sensing, John Wiley and Sons, pp. 66-106.